Interaction of CO with Gold in an Electrochemical Environment

Vijay, Sudarshan; Hogg, Thomas V.; Ehlers, Johan; Kristoffersen, Henrik H.; Katayama, Yu; Shao Horn, Yang; Chorkendorff, Ib; Chan, Karen; Seger, Brian

Published in:
Journal of Physical Chemistry C

Link to article, DOI:
10.1021/acs.jpcc.1c04013

Publication date:
2021

Document Version
Publisher's PDF, also known as Version of record

THE JOURNAL OF PHYSICAL CHEMISTRY C
A JOURNAL OF THE AMERICAN CHEMICAL SOCIETY

pubs.acs.org/JPCC

Article

Interaction of CO with Gold in an Electrochemical Environment

Sudarshan Vijay, Thomas V. Hogg, Johan Ehlers, Henrik H. Kristoffersen, Yu Katayama, Yang Shao Horn, Ib Chorkendorff, Karen Chan,* and Brian Seger*

Cite This: *J. Phys. Chem. C* 2021, 125, 17684–17689

Read Online

ACCESS | Metrics & More | Article Recommendations | Supporting Information

ABSTRACT: We present a joint theoretical–experimental study of CO coverage and facet selectivity on Au under electrochemical conditions. With in situ attenuated total reflection surface-enhanced IR spectroscopy, we investigate the CO binding in an electrochemical environment. At 0.2 V versus SHE, we detect a CO band that disappears upon facet-selective partial Pb underpotential deposition (UPD), suggesting that Pb blocks certain CO adsorption sites. With Pb UPD on single crystals and theoretical surface Pourbaix analysis, we eliminate (111) terraces as a possible adsorption site of CO. Ab initio molecular dynamics simulations of explicit water on the Au surface show the adsorption of CO on (211) steps to be significantly weakened relative to the (100) terrace due to competitive water adsorption. This result suggests that CO is more likely to bind to the (100) terrace than (211) steps in an electrochemical environment, even though Au steps under gas-phase conditions bind CO* more strongly. The competition between water and CO adsorption can result in different binding sites for CO* on Au in the gas phase and electrochemical environments.

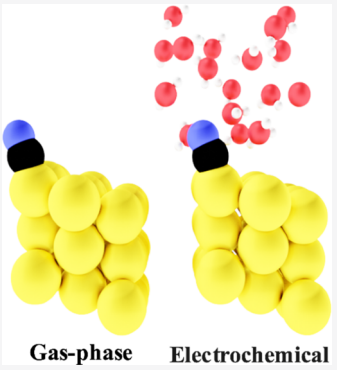

INTRODUCTION

Gold nanoparticles are highly active catalysts for a variety of thermal and electrocatalytic reactions. As a thermal catalyst, Au is excellent for CO oxidation,[1] whereas under electrochemical conditions, Au is the most active catalyst for CO_2 reduction (CO_2R) to CO and is among the most active catalysts for CO and alcohol electro-oxidation.[2] Despite the apparent simplicity of many of these reaction processes, their mechanisms remain contentious.[3−7] The determination of relevant adsorbate coverages in situ, especially under electrochemical conditions, remains an open challenge. Computational mechanistic investigations have recently begun to include the impact of solvation and field, which can have a critical impact on reaction energetics.[8−11]

This work presents a combined theoretical and experimental investigation of the binding characteristics of CO on Au under electrochemical conditions. To investigate the adsorption sites in an electrochemical environment, we performed surface-enhanced IR spectroscopy on polycrystalline gold and detected a CO band with a signal maximum at 0.2 V versus SHE. This band disappears in the presence of lead, which we attribute to the disappearance of the signal to cause blocking of the CO adsorption sites. Using cyclic voltammograms (CVs) of lead underpotential deposition (UPD) on single crystals along with computational Pourbaix analysis, we narrow the adsorption site possibilities to open motifs such as (100) terraces or (211) and (110) steps. To gain further insights into which sites could adsorb CO in an electrochemical environment, we perform density functional theory (DFT) calculations in the gas phase and in the presence of an explicit solvent. In vacuum, DFT calculations and temperature-programmed desorption spectra[12] show CO to bind more strongly on steps. In contrast, ab initio molecular dynamics simulations on (100) and (211) surfaces with explicit water suggest that competitive adsorption of water significantly destabilizes CO on the (211) step, making it more likely to bind to the (100) *terrace* instead of the (211) step. This analysis demonstrates the need to consider the effect of competitive adsorption of water since Au and other transition metals may not bind CO on the same sites in the gas phase and electrochemical environments.

RESULTS AND DISCUSSION

CO Adsorption with Lead UPD. To probe the adsorption of CO under an electrochemical environment, we performed in situ attenuated total reflection surface-enhanced IR spectroscopy (ATR-SEIRAS) in conjunction with Pb UPD on an electroless-deposited polycrystalline Au film in a 0.1 M $HClO_4$ electrolyte (see details in Supporting Information Note 1). The spectro-electrochemical cell was initially purged with 1 bar of Ar, and a spectral background was acquired. The cell was then purged with 1 bar of CO. This procedure resulted in a single vibrational band for CO adsorbed on Au at 2128 cm^{-1} (at +0.634 V vs SHE). We note that CO is well known to form Ni and Fe carbonyls when transferring through stainless-steel

Received: May 5, 2021
Revised: July 20, 2021
Published: August 9, 2021

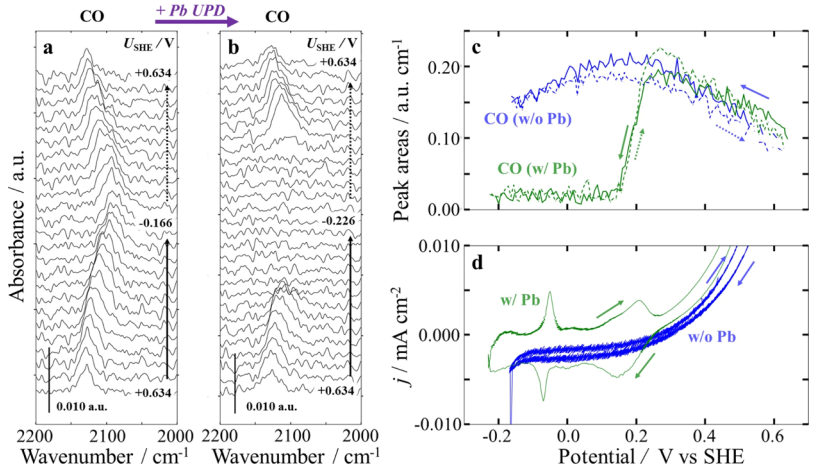

Figure 1. ATR-SEIRAS in the CO stretch region from a CV on an Au film in 0.1 M $HClO_4$ purged with 1 bar CO. A spectral background was taken at +0.634 V in Ar-purged solution. (a) ATR-SEIRAS spectra before the addition of Pb. (b) ATR-SEIRAS spectra with 1 mM $Pb(ClO_4)_2$. Every eighth spectrum is shown. (c) Integrated intensities of the CO stretch peak as a function of potential and (d) corresponding 2 mV/s CV with and without Pb.

pipes as was carried out in this work. However, the CO adsorption peak on Au at ∼2100 cm^{-1} has been shown to be present even in the absence of bubbled CO (CO was produced via electroreduction of CO_2).[13] Because of this observation, we attribute the CO adsorption peak to its adsorption on Au rather than on a Ni or Fe contaminant.

The vibrational band of CO adsorbed on Au was tracked while performing a CV in the Pb UPD region, first without Pb and then in the presence of Pb, as shown in Figure 1a,b, respectively. The observed peak position is in good agreement with the first reports of CO on vacuum and electroless-deposited Au films in $HClO_4$.[14,15] Computed CO coverage-dependent IR spectra for the (111), (100), (110), and (211) surface facets (see Figure S5) show peaks between 1900 and 2100 cm^{-1},[16,17] which is slightly smaller than the peak positions in Figure 1a,b. The linear shift in peak position with potential (i.e., the Stark shift) is measured to be 50 cm^{-1}/V, in good agreement with previous reports. The effect of adding Pb is observed as a disappearance of the CO vibration band at more cathodic potentials and the reappearance on the returning, positive-going scan. We attribute this observation to Pb deposition blocking the sites that adsorb CO. The integrated band intensities for the two cases have been coplotted in Figure 1c, illustrating the difference. Without Pb, the CO band is present in the entire potential window (+0.634 to −0.166 V) and has a maximum intensity of around 0.2 V versus SHE. In the presence of Pb, the CO band disappears over an approximately 100 mV range between 0.25 and 0.15 V vs SHE and then reappears in the same potential range on the return scan with this being a reversible process. Comparing the integrated band intensities to the UPD current in Figure 1d, we find that the disappearance of the CO band coincides with the broad and most anodic UPD waves centered around 0.2 V versus SHE. As shown in Figure 1d, the positive current which is more anodic than 0.3 V vs SHE corresponds to CO oxidation in both cases. The delayed hydrogen evolution onset in the solution with Pb allows for a slightly more cathodic potential window (+0.634 to −0.226 V vs SHE) compared to the solution without Pb.

Previously, ref 18 reported experimental Pb UPD CVs, which are reproduced in Figure 2a−d. These curves suggest that (211), (110), and (100) facets show Pb adsorption peaks at more positive potentials than the (111) surface. This trend is consistent with our computational investigations of Pb adsorption on the same facets. Pb adsorption energies were calculated on all possible adsorption sites to determine the configuration with the most stable adsorption energy (Figure S4). The half reaction for the adsorption of lead is

$$Pb^{2+} + 2e^- \leftrightarrow Pb^*$$

The free energy for this reaction as a function of potential at a given surface coverage is

$$\Delta G_{Pb} = \Delta G^0_{Pb} + 2e(U_{SHE} - U_{Pb^{2+}|Pb}) \quad (1)$$

where ΔG^0_{Pb} is the free energy referenced to 0 V versus $U_{Pb|Pb^{2+}}$, U_{SHE} is the potential referenced to the standard hydrogen electrode, and $U_{Pb^{2+}|Pb}$ is the standard redox potential of Pb^{2+}|Pb.

Figure 2a−d shows the surface Pourbaix diagrams for different coverages of Pb adsorbed on the four different surface facets of Au. Here, we assume that the entropic contribution of Pb adsorbed on Au is small, thus $\Delta G_{Pb} = \Delta E_{Pb}$. Each line corresponds to a certain coverage of Pb. On terraces, we consider coverages of 1/4, 1/9, and 1 ML (Figure 2e), and on steps, we consider coverages of 1/3, 2/3, and 1 ML (Figure 2f). Intersections between these lines are marked by the dashed black line and correspond to a change in the estimated Pb coverage on the surface and the generation of a current. The line with the lowest energy at a given potential corresponds to the estimated coverage of Pb on the Au surface.

To facilitate comparison with the experimental CVs from ref 18, we also show the computed "onsets" of the coverages considered directly on them as dashed black lines. These onsets are within the DFT error (about 0.15 eV)[19] consistent with onsets of the experimentally observed peaks. In the case of the Au(100) experiments, the multiple broadened peaks observed experimentally suggest reconstruction and the possible presence of surface defects.

With the displacement of CO* with Pb* in the CV (Figure 1d) at 0.2 V versus SHE, the surface facet(s) on which CO adsorbs must have onset potentials for Pb adsorption more positive than 0.2 V versus SHE. Both computational Pourbaix analysis and Pb UPD experiments show the onset of Pb

https://doi.org/10.1021/acs.jpcc.1c04013
J. Phys. Chem. C 2021, 125, 17684−17689

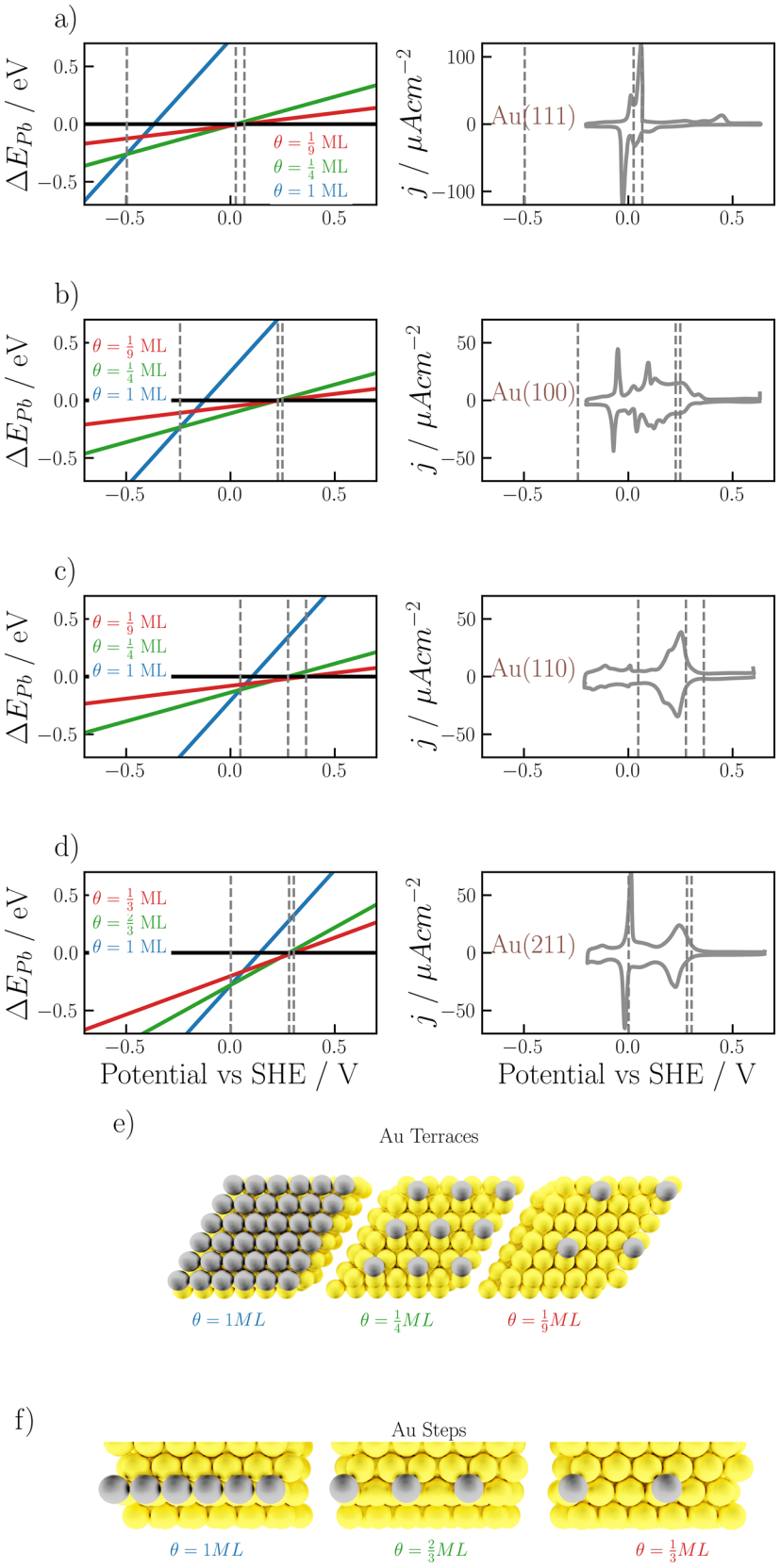

Figure 2. Computed surface Pourbaix diagrams on four prototype Au facets—(111), (100), (110), and (211). The dashed black line indicates the potential at which the coverage has increased between the discrete intervals for which the DFT calculation was performed. To the right of each surface, the Pourbaix diagram is the associated Pb-UPD CVs taken from ref 18. The multiple broadened peaks observed in the (100) facet suggest substantial reconstruction.

https://doi.org/10.1021/acs.jpcc.1c04013
J. Phys. Chem. C 2021, 125, 17684−17689

adsorption on the (111) facet to be at about 0 V versus SHE and above 0.25 V versus SHE for all other facets considered. Therefore, the combination of Pb UPD,[18] Pb adsorption calculations, and SEIRAS experiments together exclude the possibility of CO adsorption on the (111) terrace site and suggests that it adsorbs on a more open facet such as the (100) terrace and/or stepped sites.

We note that in a previous in situ STM work involving CO adsorption on Au,[20] full CO monolayer coverage on Au(111) was observed after 30 min, which is in contrast to what our work concludes. However, the authors of ref 20 saw CO depress into Au, which is highly unusual and led them to hypothesize that they were seeing physiadsorbed CO rather than chemiadsorbed CO. Thus, there could be an extra layer of complexity of CO adsorption beyond what this current work has focused on.

Electrochemical Reaction Energetics. Since steps or (100) is suggested by Pb UPD to be possible binding sites of CO* in an electrochemical environment, we now investigate the energetics of CO adsorption with ab initio molecular dynamics (AIMD) simulations with liquid water on (100) and (211), as a prototypical stepped facet.

Metal−Water Interface in Vacuum. Water has been shown to competitively adsorb to metallic surfaces, which alters the adsorption energy of small molecules.[21,22] Since an accurate description of water binding is needed to capture facet selectivity on Au in an electrochemical environment, we first evaluate the accuracy of our simulations in capturing the metal−water interaction against previously published experimental temperature-programmed desorption (TPD) of water on Au(310).[23] As a computational analogue, we consider a single layer of water on a Au(310) stepped surface with different coverages of water, as shown in Figure 3b−f, and report energies based on AIMD calculations.

Figure 3g reports the *average* adsorption energy of water $\Delta\langle E\rangle$, defined as

$$\Delta\langle E\rangle = \frac{E_{n_{H_2O^*}} - E_* - n_{H_2O^*}E_{H_2O}}{n_{H_2O^*}}$$

where $E_{n_{H_2O^*}}$ is the internal energy for a system consisting of n_{H_2O} water molecules on a surface and E_* is the internal energy of just the slab. At coverages greater than 0.5 ML, $\Delta\langle E\rangle$ is roughly constant at a value of −0.4 eV. As a basis for comparison, we use TPD experiments in ref 23, which have been analyzed using zero-order desorption kinetics. The data are reproduced in Figure 3a, where the green and red points refer to low (<1 Langmuir) and high (>1 Langmuir) exposures, respectively, and Langmuir refers to the pressure of gas (Torr) multiplied by the time of exposure (s). Two overlapping peaks were observed in the experiment between a temperature range of 158−170 K (first peak) and 161−168 K (second peak). The first peak, which we attribute to a step site, was visible at all exposures (both green and red curves in Figure 3a), while the second peak, which we attribute to a terrace site, was observed at high exposures (shown in red in Figure 3a).[23] Using leading edge analysis, where the log of the rate from a TPD spectra is fit to $1/T$, the averaged adsorption energy of water was determined to be −0.49 eV for the first peak and −0.57 eV for the second.[23] The free energies obtained from the simulations shown in Figure 3g for water coverages between 0.25 and 0.75 ML (depicted schematically

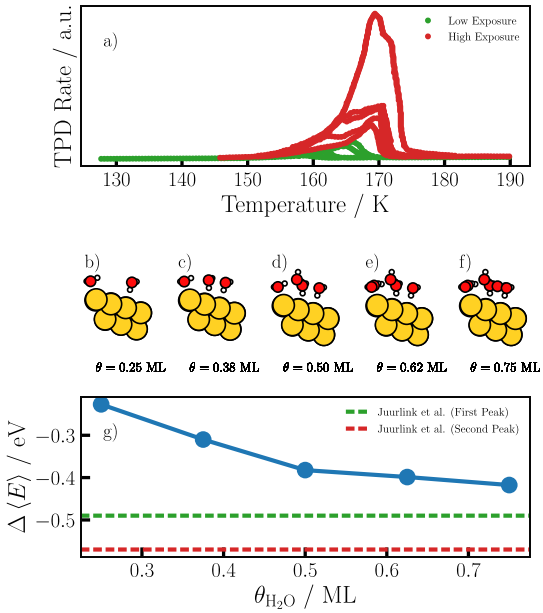

Figure 3. (a) Water adsorption TPD experiments reproduced from ref 23, where red points denote exposure greater than 1 L and green points have exposures lower than 1 L; (b−f) schematic illustrates the number of water molecules used for each coverage. (g) Average adsorption energy of H_2O on Au(310) computed using ab initio molecular dynamics simulations; experimentally determined values of the adsorption energy from ref 23 are indicated by the red and green dashed lines corresponding to high exposure (second peak) and low exposure (first peak).

in Figure 3b−f) are within 0.1 eV from the energy of the first peak, which suggests that our chosen computational setup accurately models water−Au interactions (within the typical DFT error of 0.15 eV).[19]

Metal−Water−CO Interface under Electrochemical Conditions. We now compare the computed binding strengths of CO in vacuum against those from AIMD simulations that include explicit consideration of the water, which represents the electrochemical environment. We examine the (100) and (211) surface facets as prototype open facets suggested by Pb UPD experiments to be possible binding sites of CO*. The potential range of the SEIRAS experiments (Figure 1c) is close to the potential of zero charge (pzc) of Au (0.4 V vs SHE, see Supporting Information Note 5) where electric fields and excess ion concentrations are the smallest.[9,24,25] We examined the impact of the electric field within this potential range in Figure S9, and, as expected, found it to be negligible (∼0.1 eV in a 0.5 V range). Therefore, we did not consider the impact of ions in this study.

Figure 4 shows both the adsorption energies of CO in vacuum versus AIMD calculations with explicit water. Electronic energies (ΔE) correspond to the cumulative average from AIMD trajectories, while free energies include entropic contributions from CO* and $CO_{(g)}$ using the harmonic approximation.

$$\Delta G_{CO^*} = \Delta E_{CO^*} - T(S^{harm}_{CO^*} - S^{ideal}_{CO_{(g)}}) - T\Delta S^{config} \quad (2)$$

The standard deviation associated with AIMD trajectories on the surface facets is about 0.1−0.3 eV, which compounds the errors associated with GGA functionals. We report standard deviations based on different calculation trajectories.

https://doi.org/10.1021/acs.jpcc.1c04013
J. Phys. Chem. C 2021, 125, 17684−17689

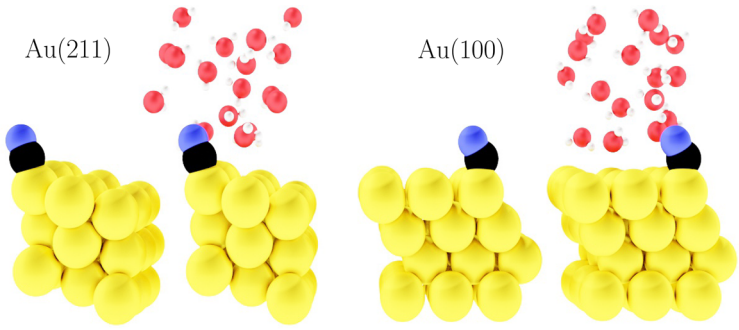

Figure 4. Snapshots of CO on Au(211) and Au(100) in vacuum or with explicit water from an ab initio MD simulation, performed in periodic unit cell sizes of 3 × 3 for (211) at a coverage of 1/3 ML and 3 × 4 for (100) at a coverage of 1/16 ML. Internal (ΔE_{CO^*}) and free energies of adsorption (ΔG_{CO^*}) with their standard deviations based on different runs are given below the snapshots.

In the gas phase, less-coordinated surfaces bind CO stronger,[26] as illustrated with the 0.17 eV smaller DFT-computed ΔG_{CO^*} for the stepped (211) and terrace (100) in vacuum, in Figure 4. The solvation energy of CO captures the difference between the energies in vacuum and in AIMD with explicit water. In the case of (211), the calculated solvation energy is large and destabilizing (0.75 eV) due to competitive water adsorption. On a flat surface like (100), there is less competition from water, which is reflected in a stabilizing solvation energy of −0.18 eV, which could arise from a stabilizing interaction of CO with the solvent (Figure S11). The significant destabilization of the adsorbed CO in water versus vacuum environments has also been observed on Cu(211)[21] and Pt(111)[22,27] (see Supporting Information Note 5).

The large difference in solvation energy between Au(211) and Au(100) gives rise to Au(100) having an ∼0.8 eV smaller ΔG_{CO^*} of 0.05 ± 0.31 eV, which suggests that Au(100) is more likely to bind CO in an electrochemical environment, although the uncertainties with the computed ΔG_{CO^*} are large. These results suggest that the competitive adsorption of water affects the adsorption energies of CO on different facets of Au differently, such that CO binds to different sites in an electrochemical environment than in vacuum. Beyond these uncertainties, GGA-DFTs may be underestimating CO* binding by about 0.1 eV on this surface, as was shown for the $(211)_{step}$ in ref 12. Despite these possible errors, ΔE_{CO^*} = −0.52 eV on Au(100) from the AIMD calculations compares well against measured enthalpy of CO adsorption on polycrystalline Au in an electrochemical environment, which was estimated to be −0.35 eV[16] for CO(aq) → CO* and −0.1 eV for CO(g) → CO(aq).[28]

CONCLUSIONS

CO adsorption on Au is a particularly important reaction for several electrochemical processes and more broadly for heterogeneous catalysis. However, there is still controversy regarding the adsorption of CO in electrochemical environments. In this study, we use a joint experimental and theoretical approach to elucidate binding characteristics of CO on Au with SEIRAS in conjunction with Pb UPD and ab initio molecular dynamics. Lead UPD in conjunction with SEIRAS suggests that open facets such as (100) and stepped sites are more likely to bind CO than (111) terraces. While Au steps bind CO* stronger than terraces in vacuum, ab initio MD simulations suggest that competitive water adsorption leads to a much larger destabilizing effect on the adsorption energies of CO on a (211) step versus a (100) terrace, making CO more likely to bind to the latter. Thus, CO can bind to different sites in the gas phase and electrochemical environments.

ASSOCIATED CONTENT

Supporting Information

The Supporting Information is available free of charge at https://pubs.acs.org/doi/10.1021/acs.jpcc.1c04013.

Computational and experimental methods, analysis of sampling of site dependence for CO with DFT calculations, IR spectra for CO, potential of zero charge computations, and details about AIMD convergence (PDF)

AUTHOR INFORMATION

Corresponding Authors

Karen Chan − *CatTheory, Department of Physics, Technical University of Denmark, 2800 Kongens Lyngby, Denmark;* orcid.org/0000-0002-6897-1108; Email: kchan@fysik.dtu.dk

Brian Seger − *SurfCat, Department of Physics, Technical University of Denmark, 2800 Kongens Lyngby, Denmark;* orcid.org/0000-0002-0036-095X; Email: brse@fysik.dtu.dk

Authors

Sudarshan Vijay − *CatTheory, Department of Physics, Technical University of Denmark, 2800 Kongens Lyngby, Denmark;* orcid.org/0000-0001-8242-0161

Thomas V. Hogg − *SurfCat, Department of Physics, Technical University of Denmark, 2800 Kongens Lyngby, Denmark*

Johan Ehlers − *SurfCat, Department of Physics, Technical University of Denmark, 2800 Kongens Lyngby, Denmark*

Henrik H. Kristoffersen − *CatTheory, Department of Physics, Technical University of Denmark, 2800 Kongens Lyngby, Denmark*

Yu Katayama − *Research Laboratory of Electronics, Massachusetts Institute of Technology, Cambridge, Massachusetts 02139, United States; Department of Applied Chemistry, Graduate School of Sciences and Technology for*

Innovation, Yamaguchi University, Tokiwadai, Ube 755-8611, Japan; orcid.org/0000-0002-7842-2938

Yang Shao Horn − *Research Laboratory of Electronics, Massachusetts Institute of Technology, Cambridge, Massachusetts 02139, United States; Department of Mechanical Engineering and Department of Materials Science and Engineering, Massachusetts Institute of Technology, Cambridge, Massachusetts 02139, United States;* orcid.org/0000-0001-8714-2121

Ib Chorkendorff − *SurfCat, Department of Physics, Technical University of Denmark, 2800 Kongens Lyngby, Denmark;* orcid.org/0000-0003-2738-0325

Complete contact information is available at: https://pubs.acs.org/10.1021/acs.jpcc.1c04013

Notes

The authors declare no competing financial interest.

■ ACKNOWLEDGMENTS

The authors would like to acknowledge funding from the European Union's Horizon 2020 research and innovation programme under grant agreement no. 85144 (SELECTCO2) and funding from the Villum Fonden through the VSUSTAIN project (9455). Y.K. would like to acknowledge financial support from the Japan Society for the Promotion of Science (JSPS) KAKENHI Grant-in-Aid for Early-Career Scientists (19 K15360) and JSPS Open Partnership Joint Research Projects/ Seminars (JPJSBP 120209925).

■ REFERENCES

(1) Lopez, N.; Janssens, T. V. W.; Clausen, B. S.; Xu, Y.; Mavrikakis, M.; Bligaard, T.; Nørskov, J. K. On the Origin of the Catalytic Activity of Gold Nanoparticles for Low-Temperature CO Oxidation. *J. Catal.* **2004**, *223*, 232−235.

(2) Chen, Y.; Li, C. W.; Kanan, M. W. Aqueous CO2 Reduction at Very Low Overpotential on Oxide-Derived Au Nanoparticles. *J. Am. Chem. Soc.* **2012**, *134*, 19969−19972.

(3) Rodriguez, P.; Koper, M. T. M. Electrocatalysis on Gold. *Phys. Chem. Chem. Phys.* **2014**, *16*, 13583−13594.

(4) Kwon, Y.; Lai, S. C. S.; Rodriguez, P.; Koper, M. T. M. Electrocatalytic Oxidation of Alcohols on Gold in Alkaline Media: Base or Gold Catalysis? *J. Am. Chem. Soc.* **2011**, *133*, 6914−6917.

(5) Li, J.; Li, X.; Gunathunge, C. M.; Waegele, M. M. Hydrogen Bonding Steers the Product Selectivity of Electrocatalytic CO Reduction. *Proc. Natl. Acad. Sci. U.S.A.* **2019**, *116*, 9220.

(6) Rodriguez, P.; Feliu, J. M.; Koper, M. T. M. Unusual Adsorption State of Carbon Monoxide on Single-Crystalline Gold Electrodes in Alkaline Media. *Electrochem. Commun.* **2009**, *11*, 1105−1108.

(7) Duan, Z.; Henkelman, G. Calculations of the PH-Dependent Onset Potential for CO Electrooxidation on Au(111). *Langmuir* **2018**, *34*, 15268−15275.

(8) Gauthier, J. A.; Ringe, S.; Dickens, C. F.; Garza, A. J.; Bell, A. T.; Head-Gordon, M.; Nørskov, J. K.; Chan, K. Challenges in Modeling Electrochemical Reaction Energetics with Polarizable Continuum Models. *ACS Catal.* **2019**, *9*, 920−931.

(9) Ringe, S.; Clark, E. L.; Resasco, J.; Walton, A.; Seger, B.; Bell, A. T.; Chan, K. Understanding Cation Effects in Electrochemical CO2 Reduction. *Energy Environ. Sci.* **2019**, *12*, 3001−3014.

(10) Patel, A. M.; Ringe, S.; Siahrostami, S.; Bajdich, M.; Nørskov, J. K.; Kulkarni, A. R. Theoretical Approaches to Describing the Oxygen Reduction Reaction Activity of Single-Atom Catalysts. *J. Phys. Chem. C* **2018**, *122*, 29307−29318.

(11) Kelly, S. R.; Kirk, C.; Chan, K.; Nørskov, J. K. Electric Field Effects in Oxygen Reduction Kinetics: Rationalizing PH Dependence at the Pt(111), Au(111), and Au(100) Electrodes. *J. Phys. Chem. C* **2020**, *124*, 14581−14591.

(12) Vijay, S.; Kristoffersen, H. H.; Katayama, Y.; Shao-Horn, Y.; Chorkendorff, I.; Seger, B.; Chan, K. How to Extract Adsorption Energies, Adsorbate-adsorbate Interaction Parameters, and Saturation Coverages from Temperature Programmed Desorption Experiments. **2021**, ChemRxiv:10.26434/chemrxiv.14525496.

(13) Dunwell, M.; Lu, Q.; Heyes, J. M.; Rosen, J.; Chen, J. G.; Yan, Y.; Jiao, F.; Xu, B. The Central Role of Bicarbonate in the Electrochemical Reduction of Carbon Dioxide on Gold. *J. Am. Chem. Soc.* **2017**, *139*, 3774−3783.

(14) Miyake, H.; Ye, S.; Osawa, M. Electroless Deposition of Gold Thin Films on Silicon for Surface-Enhanced Infrared Spectroelectrochemistry. *Electrochem. Commun.* **2002**, *4*, 973−977.

(15) Sun, S.-G.; Cai, W.-B.; Wan, L.-J.; Osawa, M. Infrared Absorption Enhancement for CO Adsorbed on Au Films in Perchloric Acid Solutions and Effects of Surface Structure Studied by Cyclic Voltammetry, Scanning Tunneling Microscopy, and Surface-Enhanced IR Spectroscopy. *J. Phys. Chem. B* **1999**, *103*, 2460−2466.

(16) Wuttig, A.; Ryu, J.; Surendranath, Y. Electrolyte Competition Controls Surface Binding of CO Intermediates to CO2 Reduction Catalysts. **2019**, ChemRxiv:10.26434/chemrxiv.7929038.

(17) Wuttig, A.; Yaguchi, M.; Motobayashi, K.; Osawa, M.; Surendranath, Y. Inhibited proton transfer enhances Au-catalyzed CO2-to-fuels selectivity. *Proc. Natl. Acad. Sci. U.S.A.* **2016**, *113*, E4585−E4593.

(18) Mezzavilla, S.; Horch, S.; Stephens, I. E. L.; Seger, B.; Chorkendorff, I. Structure Sensitivity in the Electrocatalytic Reduction of CO2with Gold Catalysts. *Angew. Chem.* **2019**, *131*, 3814−3818.

(19) Medford, A. J.; Wellendorff, J.; Vojvodic, A.; Studt, F.; Abild-Pedersen, F.; Jacobsen, K. W.; Bligaard, T.; Norskov, J. K. Assessing the Reliability of Calculated Catalytic Ammonia Synthesis Rates. *Science* **2014**, *345*, 197−200.

(20) Shue, C.-H.; Ou Yang, L.-Y.; Yau, S.-L.; Itaya, K. In-Situ Scanning Tunneling Microscopy of Carbon Monoxide Adsorbed on Au(111) Electrode. *Langmuir* **2005**, *21*, 1942−1948.

(21) Heenen, H. H.; Gauthier, J. A.; Kristoffersen, H. H.; Ludwig, T.; Chan, K. Solvation at Metal/Water Interfaces: An *Ab Initio* Molecular Dynamics Benchmark of Common Computational Approaches. *J. Chem. Phys.* **2020**, *152*, 144703.

(22) Kristoffersen, H. H.; Chang, J. H. Effect of Competitive Adsorption at the Interface between Aqueous Electrolyte and Solid Electrode. *ACS Symp. Ser.* **2019**, *1331*, 225−238.

(23) Van Spronsen, M. A.; Weststrate, K.-J.; Den Dunnen, A.; Van Reijzen, M. E.; Hahn, C.; Juurlink, L. B. F. Hydrophilic Interaction between Low-Coordinated Au and Water: H2O/Au(310) Studied with TPD and XPS. *J. Phys. Chem. C* **2016**, *120*, 8693−8703.

(24) Resasco, J.; Chen, L. D.; Clark, E.; Tsai, C.; Hahn, C.; Jaramillo, T. F.; Chan, K.; Bell, A. T. Promoter Effects of Alkali Metal Cations on the Electrochemical Reduction of Carbon Dioxide. *J. Am. Chem. Soc.* **2017**, *139*, 11277−11287.

(25) Hori, Y.; Wakebe, H.; Tsukamoto, T.; Koga, O. Electrocatalytic Process of CO Selectivity in Electrochemical Reduction of CO2 at Metal Electrodes in Aqueous Media. *Electrochim. Acta* **1994**, *39*, 1833−1839.

(26) Lopez, N.; Nørskov, J. K. Catalytic CO Oxidation by a Gold Nanoparticle: A Density Functional Study. *J. Am. Chem. Soc.* **2002**, *124*, 11262−11263.

(27) Kristoffersen, H. H.; Vegge, T.; Hansen, H. A. OH Formation and H2 Adsorption at the Liquid Water-Pt(111) Interface. *Chem. Sci.* **2018**, *9*, 6912−6921.

(28) Reed, J. J.; Evans, W. H.; Parker, V. B.; Schumm, R. H.; Halow, I. Digitizing "The NBS Tables of Chemical Thermodynamic Properties: Selected Values for Inorganic and C1 and C2 Organic Substances in SI Units". *J. Res. Natl. Inst. Stand. Technol.* **2020**, *125*, 1.